Phenotypic plasticity can be an evolutionary response to fluctuating environments

Paula García-Galindo[1], Sebastian E. Ahnert[1,2]
[1] *Department of Chemical Engineering and Biotechnology, University of Cambridge, Philippa Fawcett Drive, Cambridge CB3 0AS, UK*
[2] *The Alan Turing Institute, 96 Euston Road, London NW1 2DB, UK*
(Dated: October 2, 2024)

Phenotypic plasticity describes the biological observation that phenotypes arising from the same genotype may vary considerably. Here we show that phenotypic plasticity can arise in biological evolution as a response to changing environmental conditions. We use computationally tractable, yet biologically realistic phenotypes in the form of RNA secondary structures, and model plasticity by considering the Boltzmann distribution of secondary structures for a given genotype. Using evolutionary simulations we show that phenotypes of high plasticity emerge in rapidly changing environments. These phenotypes have near-equal Boltzmann probabilities of two different target structures, which are the fittest structures in the two environments between which we alternate during the evolutionary process. Plasticity therefore provides an optimal evolutionary response to fluctuating environmental conditions. Additionally, we find that solutions of high plasticity are more likely to be found for target pairs of higher structural similarity and phenotypic frequency.

I. INTRODUCTION

From global climatic changes to local fluctuations of temperature or chemical conditions, environmental shifts have continuously driven biological organisms to evolve strategies to cope with the challenges of a varying environment [1]. A substantial body of theoretical research on evolution in changing environments originates with Levins' foundational work [2], which first introduced the concept of the "fitness set" and more broadly explored how environmental fluctuations can hinder optimal adaptation to a single environment. Others have examined the impact of changing environments on performance trade-offs, using the Pareto front to describe optimal phenotypic solutions [3–5]. Further theoretical models have investigated the evolution of reaction norms, which describe a varying phenotypic response as a function of the environment [6, 7]. Such a varying phenotypic response that arises from the same genotype is often referred to as phenotypic plasticity, and is a widespread phenomenon in biology [1]. Here, we study the evolution of plasticity in a changing environment using biologically realistic phenotypes in the form of RNA secondary structures [8].

The genotype-phenotype (GP) map of RNA secondary structure has been studied extensively [9–13] and its large-scale structural properties have been characterised [14]. The nucleotide sequence represents the genotype, which is subject to mutations, while the RNA secondary structure represents the phenotype. This GP map can be computationally constructed for short RNA ($L < 100$) to limit the number of sequences (4^L) involved and to approximate the three-dimensional RNA fold by its base pairings, or secondary structure, which can be easily computed through experimentally validated folding algorithms [15], and represented in dot-bracket notation [14]. The RNA secondary structure GP map is computationally tractable while still being biologically relevant, as the biological functions that short RNA performs in the cell (e.g., tRNAs, miRNAs) are often highly dependent on the folded structure [16, 17].

The large-scale structural properties of the RNA GP map appear to hold across several other GP maps too, including the HP model of protein folding, gene regulatory networks (GRNs), and other biological systems. These properties have a direct impact on evolutionary trajectories, as the accessibility of phenotypes via mutations is strongly affected by the shape and size of neutral networks in the GP map [8, 12–14]. Additionally, the structure of GP maps results in highly navigable fitness landscapes, implying that true fitness valleys are uncommon in nature [18]. The structure of GP maps has also been linked to the ubiquity of symmetry in structural phenotypes [19].

Most of the literature on the RNA GP map only considers one phenotype per genotype, the most stable or minimum free energy (MFE) secondary structure, even though RNA has inherent phenotypic plasticity. At constant temperature, the folding process of an RNA nucleotide strand is probabilistic due to thermal fluctuations at the molecular scale, allowing the RNA strand to dynamically fold and unfold over time, switching between different structures based on their respective free energies [20]. This ability of the same sequence to adopt different structures can be crucial for RNA's cellular functions, such as its involvement in gene expression [21, 22], and a recently proposed 'Non-deterministic GP map' (ND GP map) framework aims to explicitly describe GP maps in which each genotype is mapped to a probability distribution of biological outcomes [23].

Some RNA sequences exhibit a high degree of plasticity, which means that the phenotype ensemble of probable structures consists of several low-energy folds separated by small energy gaps. Other sequences are associated with low plasticity, which corresponds to a large energy gap above the MFE structure. In previous studies on RNA secondary structure ensembles, the mutational robustness of an MFE structure has been shown to correlate with its structural similarity to other structures within the phenotype ensemble [24]. Furthermore, there is a correlation between an MFE structure and the suboptimal structures in the phenotype ensembles of one-point mutants, a relationship known as plastogenetic congruence [20]. These features help explain the reduction in plasticity observed for RNA in evolutionary simulations under constant environments [20]. This outcome is intuitive: if a biological function depends on a specific RNA structure being thermodynamically stable, it must also evolve to maintain mutational stability.

However, this raises the question whether, in fluctuating environments that may result in time-varying fitness landscapes with different fitness peaks, genotypes may benefit from the ability to display more than one phenotype, in other words, whether it might become beneficial for plasticity to evolve in changing environments. To investigate this hypothesis we measure the degree of plasticity that evolves

in an evolutionary model of RNA secondary structures with periodically switching environments, using the ND GP map for RNA of length $L = 12$ [23], which includes probabilistic folding in a many-to-many map from sequences to the Boltzmann ensembles of folds. We find that plasticity does indeed evolve in rapidly changing environments, as plasticity increases towards an optimal solution that narrows the plastic repertoire to a balanced distribution, representing equal probabilities of the two target RNA folds (see Fig.1). We show furthermore how the evolution of plasticity depends on the timescale of environmental change, the sampling frequency of the phenotypic distribution, and the generational timescale and mutation rate of evolution, as well as properties of the time-varying evolutionary target structures.

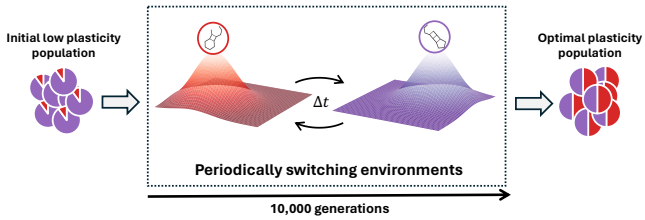

FIG. 1. **Outline of the evolutionary RNA model.** Individual pie charts represent genotypes and the associated relative Boltzmann probabilities of the two target phenotypes, T_0 (red) and T_1 (purple). The initial population (left) undergoes evolution for 10,000 generations under periodically changing environmental conditions, implemented by two alternating fitness landscapes in which the respective fitness peaks correspond to the two target structures T_0 and T_1. The switch occurs every Δt generations. We investigate whether this process results in genotype plasticity, in the form of an equal representation of the target structures in the Boltzmann ensemble.

II. METHODS

A. The RNA non-deterministic genotype-phenotype map

The RNA ND GP map maps all possible RNA sequences of a fixed length to their respective Boltzmann ensembles of secondary structures represented in dot-bracket notation, and connects each sequence to its one-mutation neighbours to form a graph in which sequences are the nodes [23]. The phenotype associated to each genotype will be the Boltzmann ensemble found for a certain energy range (so that as $\Delta E \to 0$ only the MFE remains), and the Boltzmann probabilities are normalised for that set of structures [23]. Therefore, each sequence g folds to a secondary structure p with a certain Boltzmann probability $P(p|g) = \exp((G_{ens} - G_p)/kT)$, where G_{ens} is the ensemble free energy ($G_{ens} = -kT \cdot \ln Z$ with partition function Z) and G_p is the free energy that corresponds to structure p [20]. In other words, at any point in time in an RNA population of genotype g, the number of RNAs that fold to a certain phenotype p will be proportional to the Boltzmann probability $P(p|g)$. In this study, we fix the RNA length to $L = 12$, so we construct the RNA12 ND GP map. For each RNA nucleotide sequence, the secondary structure ensemble, its ensemble free energy, and the free energy of each structure within the ensemble are computed using the `ViennaRNA subopt` [15] function set to default parameters (e.g. temperature $T = 37°$C) and energy range above the minimum free energy as $\Delta E = 15k_BT$, like in previous works [23].

B. Target secondary structures

To select target secondary structure pairs $\{T_0, T_1\}$ for periodic switching during an evolutionary simulation, we categorise the pairs based on the phenotypic frequencies or neutral space sizes NSS of the respective targets in the RNA12 ND GP map, as well as their structural difference measured in terms of their Hamming distance to each other.

First we categorise all the possible secondary structures of the RNA12 ND GP map in terms of their NSS: large ($\propto 10^5$) and small ($\propto 10^3$). We then compute all the possible target pairs that result from pairing secondary structures within and between these two NSS size categories, and therefore bin the target pairs into three NSS pair categories: both large, mixed (i.e. one large, one small), and both small. For each target pair in each category, the Hamming distance between targets is calculated, where the Hamming distance between two secondary structures of length L is calculated using $H(p_0, p_1) = 1 - \sum_j^L \delta(p_0^{(j)}, p_1^{(j)})/L$, with $p^{(j)}$ being a nucleotide base in dot-bracket notation and in our case $L = 12$. We then bin the pairs in each NSS category by their Hamming distance H: large $H \in [0.58, 1.0]$, medium $H \in [0.33, 0.58]$, and small $H \in [0, 0.33]$.

C. Genotype populations

Using a specified target secondary structure pair $\{T_0, T_1\}$ we define *plastic* genotypes, *optimal plasticity* genotypes, and *low plasticity* genotypes. A plastic genotype is one that contains both targets in its Boltzmann ensemble. An optimal plastic genotype is one with target Boltzmann probabilities $(P_0, P_1) = (0.5, 0.5)$, which represents the midpoint of the Pareto front connecting the archetypes, $P_{0,max} = (1.0, 0.0)$ and $P_{1,max} = (0.0, 1.0)$ [4]. A low plasticity genotype of either target is one that maximises the probability of adopting that target structure among all the plastic genotypes.

D. Evolutionary dynamics

Starting with a specified target pair $\{T_0, T_1\}$ and a homogeneous low plasticity genotype population of size $N = 100$, we navigate the sequence space of the RNA12 ND GP map over time through mutations and sampling from the Boltzmann ensembles of mutated sequences to generate phenotypes that then undergo a selection process. The evolutionary dynamics follow the classical haploid Wright-Fisher model [25], where in each generation a a fixed-size genotype population undergoes point mutations with a mutation rate μ (probability of a mutation happening per genotype base at each generation step) and genotypes are selected with replacement using roulette-wheel selection, where the probability of being chosen is proportional to their fitness. To evolve RNA in changing environments we periodically switch between the fitness landscapes of the two target structures with a switching frequency of $1/\Delta t$, meaning a switch occurs after a time interval Δt.

During each target epoch, the target secondary structure is assigned a maximum fitness value of $f = 1.0$, while the

fitness of other secondary structures is determined by the Hamming fitness $f_i = H(p_i, p_T)$, where p_i is the secondary structure for which fitness is being calculated, and p_T is the target secondary structure, both represented in dot-bracket notation. A fitness landscape is constructed by assigning Hamming fitness values to all phenotypes in the RNA12 ND GP map relative to a specific target structure. For each genotype, a set of N_p secondary structures is sampled from its Boltzmann ensemble, with each fold assigned a corresponding Hamming fitness value. The genotype's fitness is then defined by the highest fitness value among the sampled phenotypes, effectively giving the genotype N_p opportunities to find the optimal solution within a given time frame. This approach is not only a modeling choice but is also grounded in the biophysics of RNA interactions, where proteins may bind to natural RNAs that adopt specific conformations from an ensemble of possible structures [26].

We used simulations that run for $t = 10,000$ generations, and all evolutionary trajectories are averages computed from sample sizes of $N_s = 100$ simulations. The evolutionary dynamics simulation is summarised in the following steps:

0.0 Fix parameters μ, Δt and N_p.

0.1 Generate initial low plasticity population that maximises P_1 (P_0).

0.2 Set target to T_0 (T_1).

1.1 For each genotype in the population, sample a number N_p of folds from the phenotype Boltzmann ensemble determined by the RNA12 ND GP map.

1.2 Assign Hamming fitness, $f_i = H(p_i, p_T)$, with respect to the target fold p_T to each sampled secondary structure.

1.3 Assign fitness of each genotype to be the maximum fitness in its N_p set.

2. Generate a new population by sampling with replacement N genotypes with probability proportional to the fitness, $P_i = f_i / \sum_i^N f_i$.

3. For each base position j in each genotype i, apply a random mutation with a Bernoulli probability μ (the point mutation rate). When a mutation occurs at g_i^j, a random base different from the current one is chosen from $\{A, C, G, U\}$ with uniform probability.

4. Increase the generation time by one step, $t \to t + 1$, and set the mutated population as the updated population for t.

5. Repeat steps **1-4**, and at each Δt generation steps implement a switch to the alternative target $T_0 \leftrightarrow \mathrm{T}_1$.

6. End simulation at $t = 10,000$.

III. RESULTS

A. Optimal plasticity evolves in rapidly switching environments

We now set out to measure the prevalence of plastic phenotypes across a wide range of values of the parameters μ and Δt, and a variety of target pairs at different Hamming distances and neutral spaces of varying size. We illustrate the evolutionary simulations and the measurements of plasticity across different μ and Δt in Fig.2 through an example target pair $\{T_0^*, T_1^*\} = \{$`.((....))...`$,$`...(((...)))`$\}$, where both targets are relatively different (large Hamming distance between them, $H = 0.83$) and both are common in the GP map (large neutral space sizes). The initial low plasticity population of size $N = 100$ was chosen such that P_1 is maximised: `AUCGGCCGGGCC` with $\{P_0, P_1\} = \{0.001, 0.893\}$ (see Methods), and the fitness sampling number is $N_p = 10$ (see Section D).

The time series in Fig.2A shows the evolution of abundances and mean fitness for $t = 10,000$ generations for different values of the mutation rate μ and switching time Δt. The abundances correspond to the plastic genotypes, x_p (orange), with both targets in their phenotype ensembles; the genotypes with only the targets T_0 or T_1 in their phenotype ensembles, x_{T_0} (red) and x_{T_1} (purple); and finally the other possible genotypes x_0 (brown), which are treated as noise.

There is a noticeable increase in plastic genotypes and fitness at high switching frequency (low Δt). In Fig.2B, two examples are picked from Fig.2A to show the impact of two different switching frequencies on the initial behaviour of the plastic genotypes' abundance. Both cases have mutation rate $\mu = 0.001$, while (i) has $\Delta t = 25$ and (ii) has $\Delta t = 100$. The simulation starts at T_0 region, so we expect the T_0 population abundance to increase with the mean fitness. However, in (i) of low Δt the population of x_p quickly adapts.

To validate that generally a high switching frequency makes the plastic genotype population adapt, we compute the plastic abundance ratio: $R_p = x_p/(x_{T_0} + x_{T_1} + x_0)$, which is a ratio of the accumulated abundance from the midpoint of the simulation until the end, of the plastic abundance x_p over the rest of genotypes. We assume the midpoint as a reasonable time proxy at which the time series stabilises, thereby avoiding the computational expense of computing the exact stationary state for each simulation, while being consistent throughout the analysis.

We define the plastic population as adapted if $x_p > 0.5$, so if $R_p > 1$ the plastic genotypes have adapted, but if $R_p < 1$ the rest of the genotypes dominate. For the previous example, we show different $R_p(\mu, \Delta t)$ in Fig.2C, in which we observe that for a fixed μ, decreasing Δt leads to an increase in R_p, in other words faster switching between environments increases the prevalence of plasticity. In addition, Fig. 2C shows a positive correlation (Pearson $r = 0.75$) between R_p and mean fitness $\bar{f}$, verifying that the plastic population allows quick access to the target secondary structure.

After having established the prevalence of plasticity under certain conditions we now investigate the degree of plasticity, by analysing the population averages of the target Boltzmann probabilities $\bar{P}_0$ and $\bar{P}_1$. We show the evolution for examples (i) and (ii) in Fig.2D, where the Pareto front in the phase diagram of ($\bar{P}_0$,$\bar{P}_1$) is the line connecting the archetypes $\bar{P}_{0,max} = (1.0, 0.0)$ and $\bar{P}_{1,max} = (0.0, 1.0)$, points that represent maximum fitness in each respective target fitness landscape. Since both targets equally contribute to the evolutionary process, the optimal phenotype on the Pareto front is located at the midpoint of the line connecting the two archetypes [4]. To verify that high switching frequency leads the genotypes towards op-

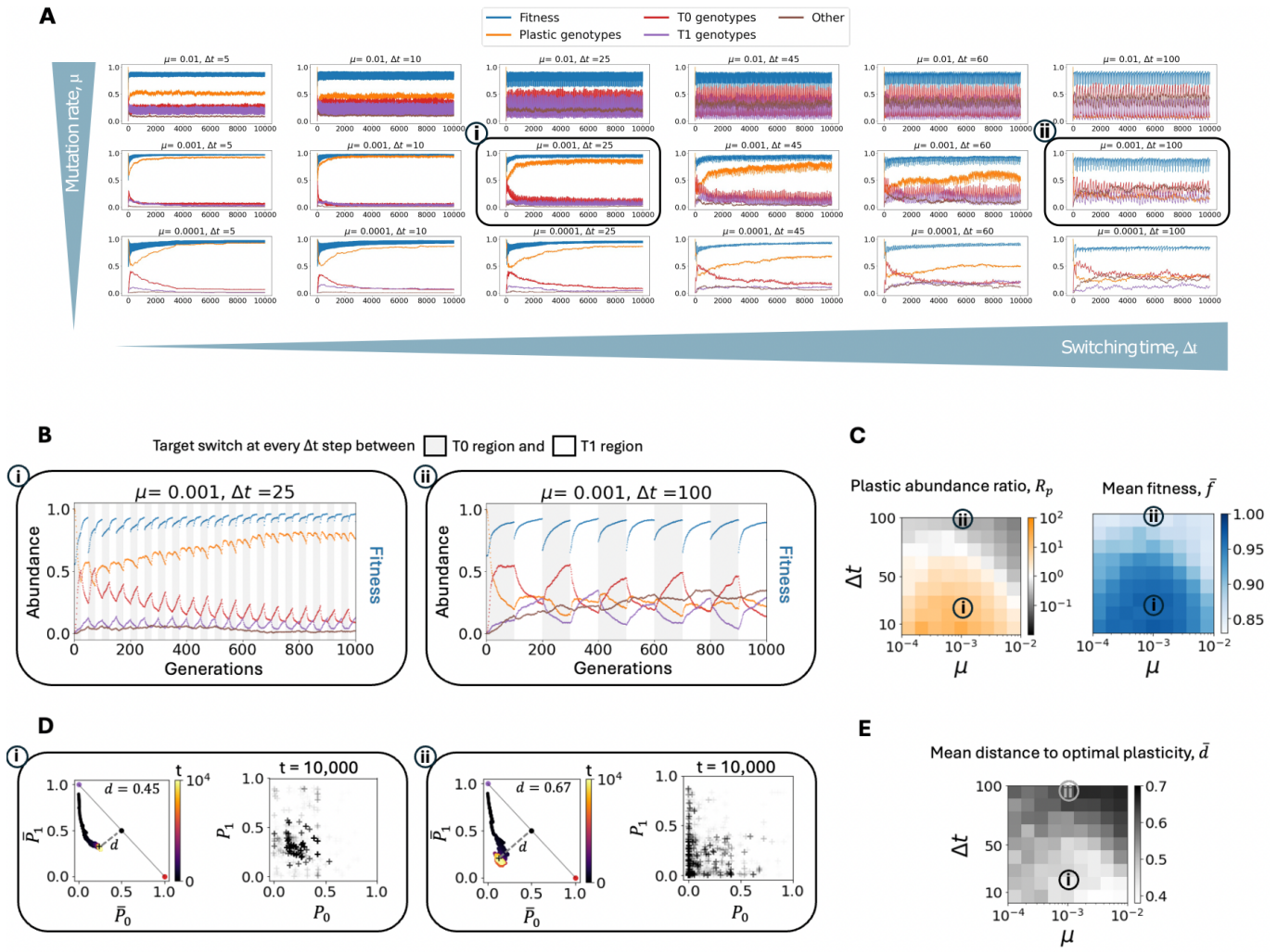

FIG. 2. **The evolution of plastic genotypes depends on the mutation rate and switching time in periodically changing environments.** Simulations are shown for target pair $\{T_0^*, T_1^*\} = \{\texttt{.((....))...}, \texttt{...(((...)))}\}$. These targets have a large Hamming distance, $H = 0.83$, and large neutral space sizes, ranked 12th and 6th, respectively, out of the total 271 in the RNA12 ND GP map [23]. The initial population maximises P_1: `AUCGGCCGGGCC` with $\{P_0, P_1\} = \{0.001, 0.893\}$. **(A)** Time series of the evolutionary dynamics in different mutation rates μ and Δt switching times. The x-axis of each subplot is time t generations up to $10,000$ and the y-axis is the abundance of the different species and the mean fitness value. Species are divided into plastic genotypes with both targets in Boltzmann ensemble, the genotypes with only T_0 or only T_1 in their ensembles, and the other genotypes are treated as noise. **(B)** shows enlarged versions of two plots in (A), marked (i) and (ii) for the time range $t = 0$ to $t = 1,000$. The grey (white) region highlights the switching time corresponding to each target $T_0(T_1)$. The regions switch every Δt. **(C)** Parameter sweep heat maps for different $(\mu, \Delta t)$ of the plastic abundance ratio R_p and of the mean fitness $\bar{f}$. These quantities are time averages from the midpoint to end of the simulation. The heat maps have a strong positive correlation of Pearson $r = 0.75$. The map for R_p shows that plasticity is prevalent (Plastic abundance ratio $> 1 =$ orange shades) for a wide range of mutation rates μ and relatively fast switching, $\Delta t < 50$. The specific simulations (i) and (ii) of $(\mu, \Delta t) = (0.001, 25)$ and $(\mu, \Delta t) = (0.001, 100)$ respectively are highlighted on the maps. **(D)** shows the evolution over time of the degree of plasticity as measured by the mean target Boltzmann probabilities $(\bar{P}_0, \bar{P}_1)$ of the population, for simulations (i) and (ii), and the mean distance d at $t = 10,000$ to the Pareto front midpoint which represents optimal plasticity. The scatter plots are accumulations of 100 simulations of the $N = 100$ population size Boltzmann probabilities at the endpoint of the simulations ($t = 10,000$), and has `alpha=0.01` so that the darker regions indicate higher density of points. Simulation (i) exhibits a much higher degree of plasticity as the $(\bar{P}_0, \bar{P}_1)$ ends up much closer to the point of optimal plasticity, and the population is clustered around this end point. By contrast the final population in (ii) is much closer to the axes, indicating a low degree of plasticity and dominance of a single phenotype. **(E)** shows the parameter sweep heat map for different $(\mu, \Delta t)$ of the mean distance $\bar{d}$ to optimal plasticity from the midpoint to the end of the simulation. This demonstrates a high degree of plasticity among the plastic phenotypes across the same wide range of μ and Δt. There is a strong negative correlation with the plastic abundance ratio (C1), Pearson $r = -0.63$, and mean fitness (C2), Pearson $r = -0.86$.

timal plasticity, we compute the normalised Euclidean distance $d = \sqrt{(\bar{P}_0(t) - 0.5)^2 + (\bar{P}_1(t) - 0.5)^2}/\sqrt{2}$, from the last point $(\bar{P}_0(t), \bar{P}_1(t))$ where $t = 10,000$, to the midpoint $(0.5, 0.5)$. As expected, both examples (i) and (ii) get closer to the optimal point, and example (i) is closer to the midpoint than example (ii). The distribution of target probabilities at $t = 10,000$ of the genotype population is shown for all $N_s = 100$ simulations, verifying that probabilities in (i) are localised closer to the midpoint, while the ones in (ii) are localised on the axis. Finally, we verify that the conditions that maximise plasticity (minimise d) correlate with maximising the plastic population abundance and the mean fitness: the parameter sweep of the time averaged distance $\bar{d}$ is shown in Fig. 2E, and has Pearson $r = -0.63$

with R_p and Pearson $r = -0.86$ with $\bar{f}$ in Fig.2C.

Fig.3A summarises these measurements of plasticity across different target pairs for each of the 9 categories that combine ranges of Hamming distance and neutral space sizes of the RNA12 ND GP map (see Methods). In Fig.3A each colour represents a category, and each point is the average of all $n = 100$ points accumulated from $R_p(\mu, \Delta t)$, where Δt is fixed. This average is calculated using the same set of 10 different μ values for each of the randomly selected 10 target pairs in a category, $\bar{R}_p = \frac{1}{n}\sum_\mu R_p(\mu, \Delta t)$. Each category of target pair shows a decrease in plasticity abundance as the switching time increases, even below the line that indicates the adapted plastic regime.

B. Plasticity maximises at different mutation rates depending on targets' structural similarity

The ND GP map can be conceptualised as overlapping clouds of secondary structure neutral spaces. For a population to evolve a plastic solution for a particular target pair, the two target folds must have neutral spaces that are sufficiently large to overlap in the ND GP map. In the case of the RNA ND GP map, a lower Hamming distance between two structures implies greater neutral space overlap [20, 24]. Thus, for target pairs with sufficiently large neutral spaces, greater structural differences result in less overlap between these spaces. Consequently, for the population to find the optimal plastic solution, it must navigate the ND GP map in large steps, i.e., with a high mutation rate, to avoid getting trapped in local maxima (exploration catastrophe), but not so large that it exits the region of neutral space overlap (error catastrophe). However, if the structures are similar, localised regions of plasticity exist and can be more easily discovered if the evolutionary dynamics is driven by low mutation rates. To test this, we analyse target pairs with large neutral space sizes and varying Hamming distances (see Methods), as shown in Fig. 3B. Each point is the average of all $n = 100$ points accumulated from $R_p(\mu, \Delta t)$, where μ is fixed. This average is calculated using the same set of 10 different Δt values for each of the randomly selected 10 target pairs in each H category, $\bar{R}_p = \frac{1}{n}\sum_{\Delta t} R_p(\mu, \Delta t)$. The value of μ that maximises plasticity decreases with the Hamming distance between the targets.

C. Plasticity is more likely to evolve for similar targets of large neutral spaces

Optimal plasticity can of course only evolve if the optimal plastic genotypes are present in the ND GP map in the first place. As previously mentioned, the more common the targets are in the RNA ND GP map (large neutral spaces), and the more their neutral spaces overlap (low Hamming distance between targets), the more likely the plastic genotypes exist and therefore can be found in evolution. We test the intuition that Hamming distance and neutral space size combine to increase plasticity by analysing the plastic abundance ratio R_p for 10 different batches of 9 target pairs where each pair is randomly selected from one of the 9 different categories combining neutral space sizes NSS and Hamming distances H (see Methods). An example is shown in Fig.4A to show the parameter sweeps of R_p values at each target pair category. We observe an increase in $R_p > 1$ regions as H decreases and NSS increases, as expected. To visualise the results for the 10 different batches, the accumulated R_p values for the target pairs in the 9 different categories are represented in Fig.4B. The dotted black line is $R_p = 1$ and separates the adapted plastic (right) and non-plastic (left) R_p regions. The histogram densities in Fig.4B shift towards the plastic region for large neutral spaces and small Hamming distances. Equally, we verify that the mean fitness peaks shift towards higher values with the same trend. This pattern is also evident in the vertical ordering of the categories observed in Fig.3A.

D. Plasticity requires multiple phenotypic expressions per generation

Our fitness function allows multiple expressions of the phenotype in a given generation, through the parameter N_p. This acknowledges the difference between the generational timescale and the timescale of phenotypic production. A value of $N_p > 1$ assumes that an RNA sequence has multiple opportunities to fold, and assigns fitness based on the highest fitness observed among N_p sampled folds from the Boltzmann ensemble. The number of samples N_p reflects the selection process's leniency: if $N_p = 1$, only the first sampled fold determines the genotype's fate, whereas if $N_p \to \infty$, the sequence can access any solution within its plastic repertoire. We find that plasticity only emerges if $N_p > 1$, but that varying it beyond that does not alter the qualitative outcomes substantially (see Fig.S1 in Supplementary Material), which is why we have used a fixed value of $N_p = 10$ for most of our analyses.

IV. DISCUSSION

Our evolutionary environment varies in a very specific way, which may not represent a very realistic model of environmental change. Future research could investigate whether the ND GP map structure allows for the same qualitative results in response to more unpredictable environmental changes, such as stochastically varying conditions, and for more than two target structures, potentially leading to different optimal Boltzmann distributions. Our current results assume an initial population already containing genotypes that have both targets (plastic) but maximises the probability of either target structure. It would be valuable to study the accessibility of plastic genotypes starting from a random population that lacks one of the target structures.

Phenotypic plasticity, meaning a genotype's ability to adopt different phenotypes, is widespread in biology [27]. This phenomenon occurs at various scales and conditions, from multicellular organisms with variable traits, like leaf shape in plants, to the molecular level, where RNA and proteins change conformations. RNA, in particular, has numerous critical roles in the cell that rely on plasticity. For example, riboswitches or RNA thermometers regulate gene expression by adopting different conformations in response to ligand bindings or temperature changes, respectively [28–30]. While all RNA sequences exhibit some degree of dynamic structural change at constant temperature, our research demonstrates that this inherent RNA plasticity can be optimised and exploited as a direct evolutionary response to environmental fluctuations. A systematic search for functional RNAs that exploit this type of plasticity may be a promising avenue of inquiry.

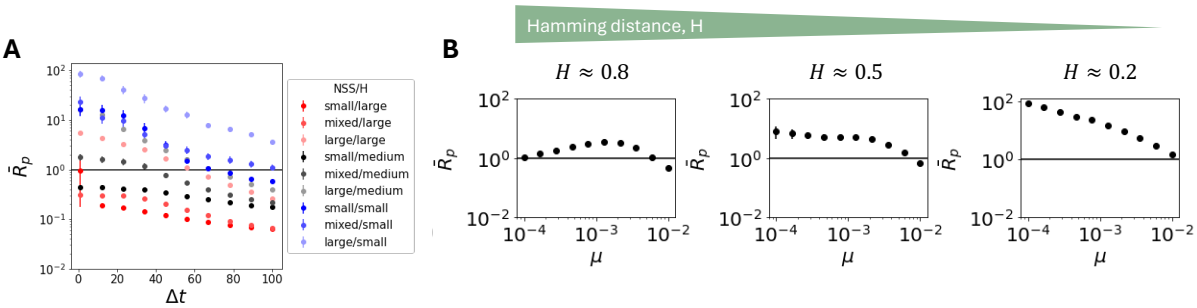

FIG. 3. **(A) Decrease in switching time increases average plastic abundance ratio.** Each point is the average of 100 points accumulated from $R_p(\mu, \Delta t)$, where Δt is fixed, calculated using the same set of 10 different μ values for each of the 10 different randomly chosen target pairs that belong to a category. The categories (see Methods) are defined by Hamming distance H (red = large, black = medium, blue = small) and neutral set size, NSS (dark hue = small, medium hue = mixed, light hue = large). **(B) Plasticity maximises at different mutation rates depending on Hamming distance between targets.** Each point is the average of 100 points accumulated from $R_p(\mu, \Delta t)$, where μ is fixed, calculated using the same set of 10 different Δt values for each of the 10 different randomly chosen target pairs from each Hamming distance H category, in particular these pairs belong to large ≈ 0.8, medium ≈ 0.5, or small ≈ 0.2 Hamming distance. Here we are only considering targets with large neutral space sizes, $NSS \propto 10^5$.

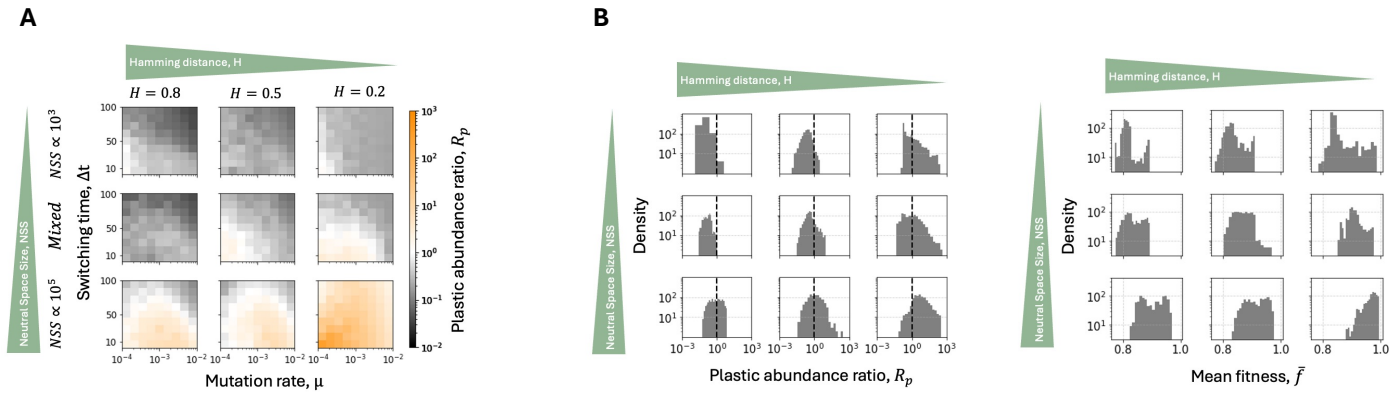

FIG. 4. **The choice of target pair has an impact in plasticity evolution determined by the ND GP map. (A)** Heat maps of parameter sweeps $(\mu, \Delta t)$ of plastic abundance ratio R_p (see Fig.2C) for different target pairs. Columns represent Hamming distance between secondary structures in each pair. The rows indicate the scale of the secondary structures' neutral space sizes NSS on the RNA12 ND GP map. The middle row represents the mixed target pairs, each pair having one target secondary structure with $NSS \propto 10^3$ and the other with $NSS \propto 10^5$. **(B)** Histograms of R_p and mean fitness $\bar{f}$ values of 10 different batches of 9 pairs, where each pair was randomly selected from one of the 9 categories of NSS and H indicated in the Methods and that align with the categories in (A), verifying that increasing NSS and decreasing H between target pairs induces more plasticity in the evolutionary dynamics of periodically switching environments.

V. Acknowledgements

We wish to thank Uri Alon for useful comments. P.G.G acknowledges "la Caixa" Foundation (Fellowship: LCF/BQ/EU21/11890140) and King's College, Cambridge for funding support.

References

[1] L. A. Meyers and J. J. Bull, "Fighting change with change: adaptive variation in an uncertain world", Trends in Ecology & Evolution **17**, Publisher: Elsevier, 551–557 (2002).

[2] R. Levins, *Evolution in Changing Environments: Some Theoretical Explorations* (Princeton University Press, Aug. 1968).

[3] E. Kussell and S. Leibler, "Phenotypic Diversity, Population Growth, and Information in Fluctuating Environments", Science **309**, 2075–2078 (2005).

[4] O. Shoval, H. Sheftel, G. Shinar, Y. Hart, O. Ramote, A. Mayo, E. Dekel, K. Kavanagh, and U. Alon, "Evolutionary Trade-Offs, Pareto Optimality, and the Geometry of Phenotype Space", Science **336**, 1157–1160 (2012).

[5] M. Tikhonov, S. Kachru, and D. S. Fisher, "A model for the interplay between plastic tradeoffs and evolution in changing environments", Proceedings of the National Academy of Sciences **117**, Publisher: Proceedings of the National Academy of Sciences, 8934–8940 (2020).

[6] L. W. Ancel, "Undermining the Baldwin Expediting Effect: Does Phenotypic Plasticity Accelerate Evolution?", Theoretical Population Biology **58**, 307–319 (2000).

[7] R. Lande, "Adaptation to an extraordinary environment by evolution of phenotypic plasticity and genetic assimilation", Journal of Evolutionary Biology **22**, 1435–1446 (2009).

[8] S. Manrubia, J. A. Cuesta, J. Aguirre, S. E. Ahnert, L. Altenberg, A. V. Cano, P. Catalán, R. Diaz-Uriarte, S. F. Elena, J. A. García-Martín, P. Hogeweg, B. S. Khatri, J. Krug, A. A. Louis, N. S. Martin, J. L. Payne, M. J. Tarnowski, and M. Weiß, "From genotypes to organisms: State-of-the-art and per-

spectives of a cornerstone in evolutionary dynamics", Physics of Life Reviews **38**, 55–106 (2021).

[9]P. Schuster, W. Fontana, P. F. Stadler, and I. L. Hofacker, "From sequences to shapes and back: a case study in RNA secondary structures", Proceedings of the Royal Society of London. Series B: Biological Sciences **255**, 279–284 (1994).

[10]P. Schuster, "Prediction of RNA secondary structures: from theory to models and real molecules", Reports on Progress in Physics **69**, 1419 (2006).

[11]A. Wagner, "Robustness and evolvability: a paradox resolved", Proceedings of the Royal Society B: Biological Sciences **275**, 91–100 (2008).

[12]S. Schaper and A. A. Louis, "The Arrival of the Frequent: How Bias in Genotype-Phenotype Maps Can Steer Populations to Local Optima", PLoS ONE **9**, e86635 (2014).

[13]S. F. Greenbury, S. Schaper, S. E. Ahnert, and A. A. Louis, "Genetic Correlations Greatly Increase Mutational Robustness and Can Both Reduce and Enhance Evolvability", PLOS Computational Biology **12**, edited by R. A. Goldstein, e1004773 (2016).

[14]S. E. Ahnert, "Structural properties of genotype–phenotype maps", Journal of The Royal Society Interface **14**, 20170275 (2017).

[15]R. Lorenz, S. H. Bernhart, C. H. z. Siederdissen, H. Tafer, C. Flamm, P. F. Stadler, and I. L. Hofacker, "ViennaRNA Package 2.0", Algorithms for Molecular Biology **6**, 26 (2011).

[16]H. Schwalbe, J. Buck, B. Fürtig, J. Noeske, and J. Wöhnert, "Structures of RNA Switches: Insight into Molecular Recognition and Tertiary Structure", Angewandte Chemie International Edition **46**, 1212–1219 (2007).

[17]M. Doetsch, R. Schroeder, and B. Fürtig, "Transient RNA–protein interactions in RNA folding", The FEBS Journal **278**, 1634–1642 (2011).

[18]S. F. Greenbury, A. A. Louis, and S. E. Ahnert, "The structure of genotype-phenotype maps makes fitness landscapes navigable", Nature Ecology & Evolution, 1–11 (2022).

[19]I. G. Johnston, K. Dingle, S. F. Greenbury, C. Q. Camargo, J. P. K. Doye, S. E. Ahnert, and A. A. Louis, "Symmetry and simplicity spontaneously emerge from the algorithmic nature of evolution.", Proceedings of the National Academy of Sciences of the United States of America **119**, e2113883119 (2022).

[20]L. W. Ancel and W. Fontana, "Plasticity, evolvability, and modularity in RNA", Journal of Experimental Zoology **288**, 242–283 (2000).

[21]N. Vaidya and N. Lehman, "One RNA plays three roles to provide catalytic activity to a group I intron lacking an endogenous internal guide sequence", Nucleic Acids Research **37**, 3981–3989 (2009).

[22]E. A. Schultes and D. P. Bartel, "One Sequence, Two Ribozymes: Implications for the Emergence of New Ribozyme Folds", Science **289**, 448–452 (2000).

[23]P. García-Galindo, S. E. Ahnert, and N. S. Martin, "The non-deterministic genotype–phenotype map of RNA secondary structure", Journal of The Royal Society Interface **20**, 20230132 (2023).

[24]S. Wuchty, W. Fontana, I. L. Hofacker, and P. Schuster, "Complete suboptimal folding of RNA and the stability of secondary structures", Biopolymers **49**, 145–165 (1999).

[25]W. J. Ewens, *Mathematical Population Genetics*, Vol. 27, Interdisciplinary Applied Mathematics (Springer, New York, NY, 2004).

[26]Q. Zhang, A. C. Stelzer, C. K. Fisher, and H. M. Al-Hashimi, "Visualizing spatially correlated dynamics that directs RNA conformational transitions", Nature **450**, 1263–1267 (2007).

[27]M. J. West-Eberhard, *Developmental Plasticity and Evolution* (Oxford University Press, Mar. 2003).

[28]M. Mandal and R. R. Breaker, "Gene regulation by riboswitches", Nature Reviews Molecular Cell Biology **5**, 451–463 (2004).

[29]J. Kortmann and F. Narberhaus, "Bacterial RNA thermometers: molecular zippers and switches", Nature Reviews Microbiology **10**, 255–265 (2012).

[30]S. E. Thomas, M. Balcerowicz, and B. Y.-W. Chung, "RNA structure mediated thermoregulation: What can we learn from plants?", Frontiers in Plant Science **13**, 10.3389/fpls.2022.938570 (2022).

Supplementary Material: Phenotypic plasticity can be an evolutionary response to fluctuating environments

Paula García-Galindo, Sebastian E. Ahnert

S1 Fitness sampling number N_p

The fitness sampling function assigns the fitness f of a genotype by sampling N_p folds p_i (where $i = 1, \ldots, N_p$) from the genotype's Boltzmann ensemble and selecting the highest Hamming fitness f_H relative to a target fold p_T from these samples:

$$f = \max\{f_H(p_1, p_T), ..., f_H(p_{N_p}, p_T)\}$$

The N_p value does not change the qualitative results described in the paper, although behaviour can differ for the most extreme case, $N_p = 1$ (navy blue colour) as shown in Fig. S1.

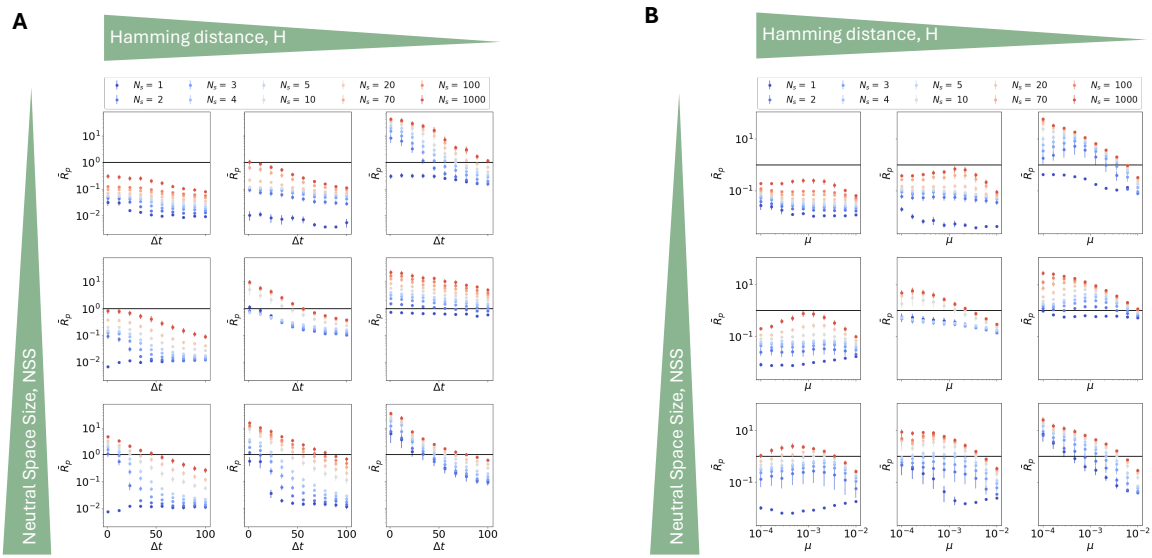

Figure S1: Change of N_p value still gives: (A) Decrease in switching time increases average plastic abundance ratio and (B) for large neutral spaces, plasticity maximises at different mutation rates depending on targets' Hamming distance Each point is an average of 10 values of R_p of 10 different (A)μ, (B)Δt and fixed (A)Δt, (B)μ from a randomly selected target pair of a particular category ordered by neutral set size, NSS, and decreasing Hamming distance, H (see Methods). Each colour corresponds to the R_p averages for a fixed N_p. The colours increase in warmth with the value of N_p. The coolest colour, navy blue, is $N_p = 1$ and warmest colour is $N_p = 1000$.